Neuron, volume 61

Electrical coupling mediates tunable low-frequency oscillations and resonance in the cerebellar Golgi cell network

Guillaume P. Dugué, Nicolas Brunel, Vincent Hakim, Eric Schwartz, Mireille Chat, Maxime Lévesque, Richard Courtemanche, Clément Léna and Stéphane Dieudonné.

Supplemental Data

Supplemental Experimental Procedures

Slices preparation

After decapitation, the cerebellum was rapidly dissected in a cold ACSF containing (in mM): 125 NaCl, 2.5 KCl, 1.25 NaH_2PO_4, 26 $NaHCO_3$, 25 glucose, 1.6 $CaCl_2$ and 1.5 $MgCl_2$, bubbled with 95% O_2, 5% CO_2. Sagittal slices 250 µm thick were cut using a Microm (Walldorf, Germany) HM650V slicer, in a cold solution with the following composition (in mM): 130 Kgluconate, 15 KCl, 0.05 EGTA, 20 HEPES and 25 glucose, titrated to pH 7.4 with NaOH and supplemented with 50 mM D-APV to prevent glutamate excitotoxicity. As explained (Dugue et al., 2005), the purpose of this solution was to limit the entry of calcium and other extracellular ions into cells whose neurites were cut. Slices were then allowed to recover in a solution containing (in mM) 225 D-Mannitol, 2.5 KCl, 1.25 NaH_2PO_4, 25 $NaHCO_3$, 25 glucose, 0.8 $CaCl_2$ and 8 $MgCl_2$ (32 °C, bubbled with 95% O_2, 5% CO_2) to help for progressive ions reequilibration toward normal external concentrations. Finally, slices were incubated in warm ACSF (32 °C, bubbled with 95% O_2, 5% CO_2) until recording.

eGFP visualization and calculation of intercellular distances

The eGFP was visualized with an epifluorescence system comprising a Roper Scientific (Trenton, NJ, USA) CoolSNAP HQ digital camera and a Sutter Instruments (Novato, CA, USA) Lambda DG-4 illumination device, both controled with the MetaMorph software (Molecular Devices, Sunnyvale, CA, USA). To calculate the intercellular distance (ID) in Golgi cells paired-recordings, a stack of fluorescence pictures was taken at 2 µm intervals

with a P-720 PIFOC piezoelectric objective focusing system (Physik Instrumente, Karlsruhe, Germany). The ID was the distance between the cell bodies along the Purkinje cell layer axis.

Phase-response curve calculation

To assess the effect of the AHP on the firing pattern of coupled cells, an AHP waveform was injected into one cell (cell 1) to evoke artificial HJPs in a coupled cell (cell 2). The AHP waveform was obtained by taking the voltage trace underneath −40 mV in the average spike of a Golgi cell firing at 13 Hz. Cell 1 was voltage-clamped at −40 mV in the presence of 2 mM QX-314 in the patch pipette and the waveform was injected at regular sweeps intervals. Tonic spiking at 10−15 Hz was induced in cell 2 by injection of steady depolarizing current. For each sweep in cell 2, the ISI during which the HJP was evoked (test ISI) was measured, as well as the average ISI over one second before the waveform injection (control ISI). Evoked HJPs occurred at random phases within the discharge cycle. The phase of the waveform injection was calculated relative to the control ISI. Phase-response curves were obtained by plotting the duration of the test ISI (% of control ISI) against the phase of the evoked ISI.

Microelectrode implantation for **in vivo** *recordings*

Sprague-Dawley male rats (400−500g) were obtained from Charles River Laboratories (St-Constant, Quebec, Canada). For electrode implantation a burr hole of 5 mm diameter was drilled above the cerebellum, using coordinates (AP, -12; Lat 3) (Paxinos and Watson, 2005). The targeted regions were the Crus II and paramedian lobules. Rats were implanted with a headstage (Neuralynx, Bozeman, MT, USA) mounted with 4 to 8 epoxylite-covered tungsten microelectrodes (0.5−4 MΩ, 75 µm, FHC Inc., Bowdoin, ME, USA) inserted in 100 µm polyimide tubes and mounted on freely moveable microdrives. Positioning with these drives, done with a microscrewdriver with a ratio of 6 turns/mm, is precise to ~20 µm (~1/8 of a turn, experimenter-bound). Electrodes were inserted in stainless steel guide tubes, organized along the anteroposterior and/or the mediolateral axis of the cerebellum. An insulated stainless steel wire (except at the tip), soldered to a stainless steel plate and attached to one of the six anchor screws was used as the ground. An insulated stainless steel wire inserted into a 100 µm polyimide tube and placed on the surface of the cortex was used as the reference.

Immunocytochemistry

In GlyT2-eGFP mice, about 20% of Golgi cells do not express GlyT2 and are thus eGFP-negative (Simat et al., 2007), but express the glutamic acid decarboxylase (GAD) and contain gamma-aminobutyric acid (GABA) (Ottersen et al., 1988). To constrain the connectivity of the model, we calculated the density of Golgi cells in cerebellar slices obtained from GlyT2-eGFP mice and stained for GABA. A mouse monoclonal antibody against GABA (3A12, 1:2000, Swant, Bellinzona, Switzerland) and a CY3 anti-mouse IgG secondary antibody (715-165-151, 1:300, Jackson ImmunoResearch, West Grove, PA, USA) were used at the indicated dilutions. Seven-month-old GlyT2-eGFP mice were perfused and sagittal slices of the cerebellar vermis (50 µm thick) were obtained and stained as described previously (Collin et al., 2005). Stained slices were examined using a 20X objective on a Zeiss (Oberkochen, Germany) LSM 510 confocal microscope equipped with two lasers: Argon multiray (used at 488 nm) and Helium (543 nm). LSM Image Browser (Zeiss) and Adobe Photoshop CS (Adobe Systems, San Jose, CA, USA) were used for image analysis and processing. Single-labelled (either GABA-positive or eGFP-positive) and double-labelled (GABA and eGFP-positive) Golgi cell somata were counted on single confocal sections taken in the first 8 µm of the slices (the zone where the antibodies had penetrated with sufficient efficacy). In GlyT2-eGFP mice, Lugaro cells, the second class of granular layer (GL) inhibitory interneurons, are also eGFP-labelled (Simat et al., 2007). Lugaro cell somata were identified by their characteristic fusiform shape and counted seperately. Stacks (n = 10) of the whole slice thickness were taken at 1 µm intervals (n = 10) to calculate the ratio R = (density of eGFP+ cells in the stack per GL mm^3) / (average number of eGFP+ cells per GL mm^2 in one optical section of the stack). To obtain the density of Golgi cells (per GL mm^3), their average number in single optical sections (per GL mm^2) was multiplied by the average value of R. This yielded a density of 9515 ± 2721 Golgi cells per GL mm^3.

Model

The model consisted of 144 neurons arranged on a 12x12 grid with 33 µm spacing. To reproduce the fluctuations in distance-dependent junctional coupling, cell positions were drawn randomly from the grid vertices, using a uniform distribution between ± 25% of grid spacing both in x and y directions. The radius of each cell was drawn randomly from 0.7 to 1.3 times the average radius (70 µm) as well as its density of processes (from 0.7 to 1.3 relative to average). The junctional conductance between cell i and j was taken proportional to

the area of overlap between the two disks and to the relative densities of processes of both cells. The normalization was chosen so that the average conductance of two cells at zero distance is 0.75 nS.

References

Collin, T., Chat, M., Lucas, M.G., Moreno, H., Racay, P., Schwaller, B., Marty, A., and Llano, I. (2005). Developmental changes in parvalbumin regulate presynaptic Ca2+ signaling. J Neurosci *25*, 96-107.

Dugue, G.P., Dumoulin, A., Triller, A., and Dieudonne, S. (2005). Target-dependent use of co-released inhibitory transmitters at central synapses. J Neurosci *25*, 6490-6498.

Ottersen, O.P., Storm-Mathisen, J., and Somogyi, P. (1988). Colocalization of glycine-like and GABA-like immunoreactivities in Golgi cell terminals in the rat cerebellum: a postembedding light and electron microscopic study. Brain Res *450*, 342-353.

Paxinos, G., and Watson, C. (2005). The rat brain in stereotaxic coordinates., 5th edition edn (Oxford, UK: Elsevier Academic Press).

Simat, M., Parpan, F., and Fritschy, J.M. (2007). Heterogeneity of glycinergic and gabaergic interneurons in the granule cell layer of mouse cerebellum. J Comp Neurol *500*, 71-83.

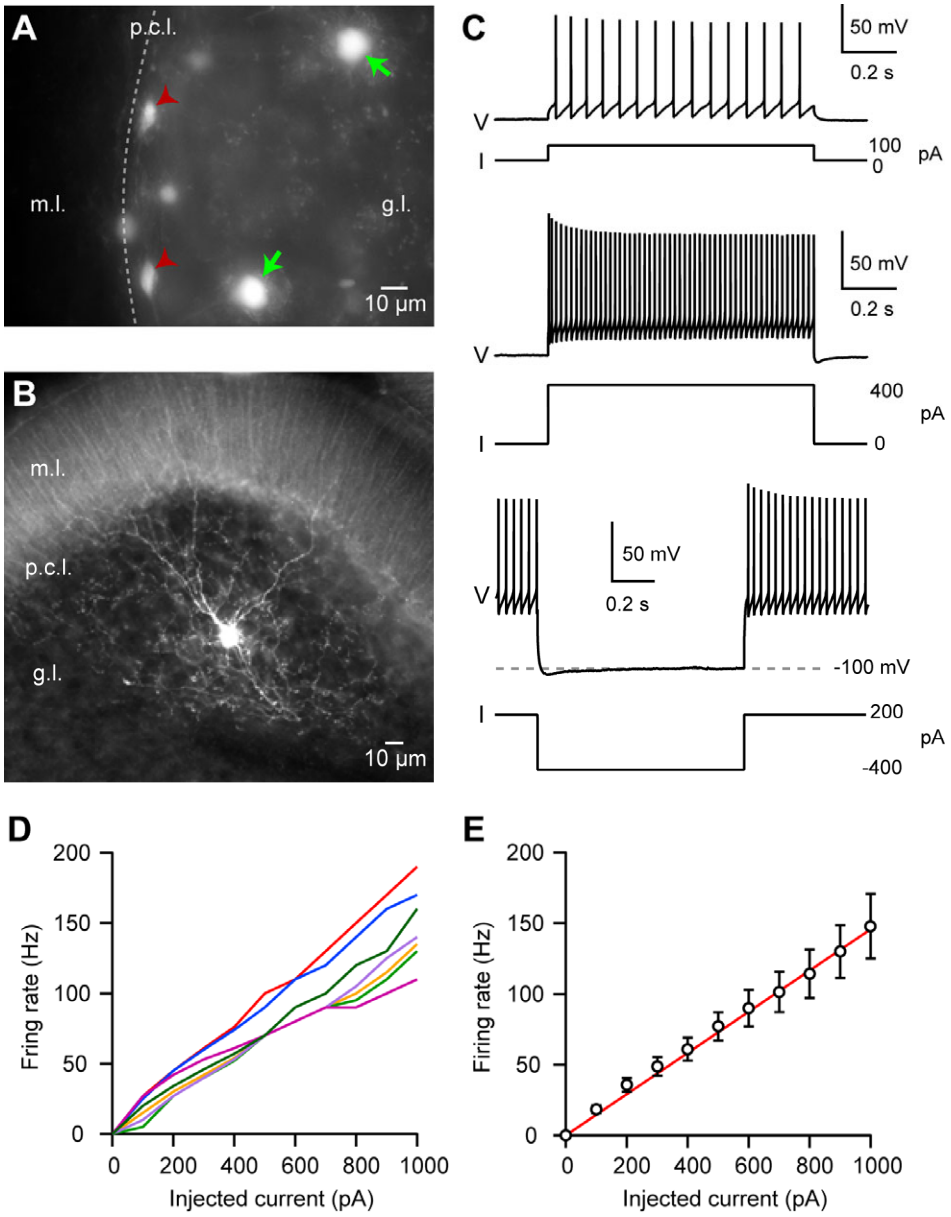

Figure S1. Response of Golgi cells to depolarizing and hyperpolarizing pulses.
(A) Epifluorescence picture of a cerebellar slice prepared from a GlyT2-eGFP mouse, showing the granular layer (g.l.), the Purkinje cell layer (p.c.l., dashed line) and the molecular layer (m.l.). Green arrows indicate Golgi cell somata. Red arrowheads indicate Lugaro cell somata. Lugaro cells can be recognized by their fusiform cell body located underneath the Purkinje cell layer. The picture is the projection of a stack of 20 images taken at 2 µm intervals. (B) Example of a recorded Golgi cell filled with 2% Neurobiotin and revealed with Streptavidin-CY3. (C) Typical response of Golgi cells to depolarizing (top and middle) and hyperpolarizing (bottom) current steps (1 s long). Note the absence of adaptation during the depolarizing steps (top and middle), and the absence of a marked rebound after the hyperpolarizing step (bottom). (D) Firing rate of 7 Golgi cells (each one represented by one color) as a function of the injected current during the depolarizing step. (E) Average firing rate (± SEM) as a function of the injected current during the depolarizing step (n = 7). The linear fit (red line) returned a slope of 14.6 ± 0.5 Hz per 100 pA.

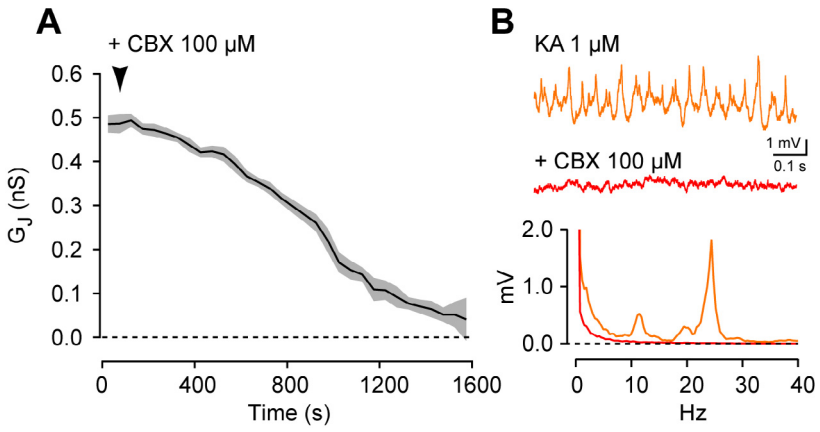

Figure S2. Gap junction blockade with carbenoxolone suppresses kainate-induced STOs in Golgi cells.
(A) Time course of the reduction of the junctional conductance (GJ) after bath application of 100 µM carbenoxolone (CBX) (example from one paired recording). Dark line: average GJ (bin = 50 s). Gray area: ± SD. (B) Top: voltage traces obtained in a Golgi cell during kainate stimulation before (orange) and 25 min after (red) CBX application. Bottom: corresponding power spectral density functions showing the total disappearance of the kainate-induced STO.

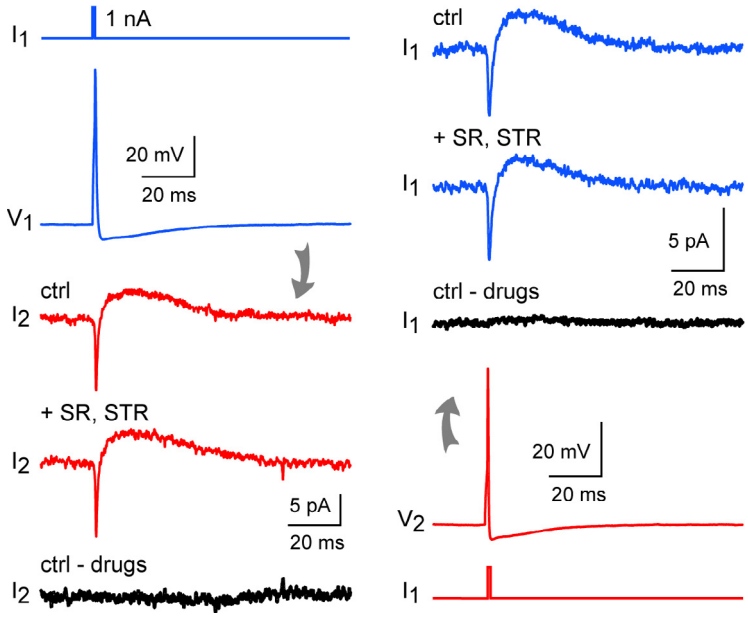

Figure S3. Absence of chemical synaptic interactions in the Golgi cell network.
Response of an electrically coupled pair to depolarizing current pulse injections (1 nA, 1 ms). The blue traces correspond to one cell (cell 1) and the red traces to the other (cell 2). Pulses were injected either in cell 1 (left) or in cell 2 (right) at resting potential while the other cell was clamped at −75 mV. The black trace was obtained by subtracting the average spikelet (obtained after blocking GABAA and glycine receptors) from the average current evoked in control conditions. Traces were averaged from 40 sweeps. In these recordings, the equilibrium potential for chloride was −39 mV.

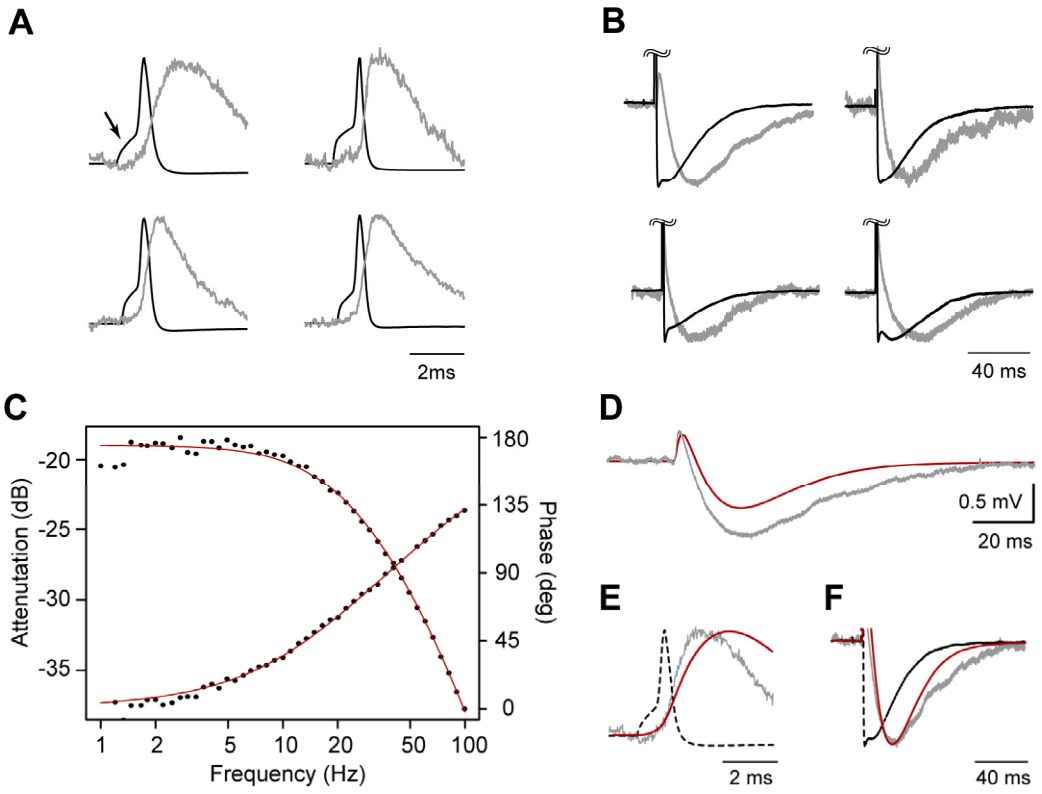

Figure S4. Relation between the pre-junctional spike and post-junctional spikelet.
(A) The spikelet peak occurs later than the prejunctional spike peak. Examples of average spikes (black) and scaled spikelets (gray) from 4 different pairs. The hump on the spike rising phase (arrow) corresponds to the brief depolarization induced by the current pulse used to trigger the spike. (B) Comparison of the time-course of the hyperpolarizing phase of the spike (black) and the scaled spikelet (gray). (C-F) Comparison of the observed spikelet and the spikelet predicted from the Bode diagram of the pair. (C) Fit of the Bode diagram with a simple model. Since the Bode diagram did not cover all the frequencies present in the spectrum of the spike, it was extrapolated using a second order linear system (time constants: 10.4 ms and 1.7 ms, red). (D) Prediction of the spikelet by the model (red) and comparison with the observed spikelet (gray). Note the slight difference in amplitude and time of peak of the DJP in the observed and predicted spikelets. The predicted amplitude of the HJP was clearly smaller than observed. (E) Time course of the DJP. The prejunctional spike is indicated in dotted line. (F) Time-course of the HJP of the predicted (red) and observed (gray) spikelet. The traces in (E) and (F) are scaled for sake of comparison.

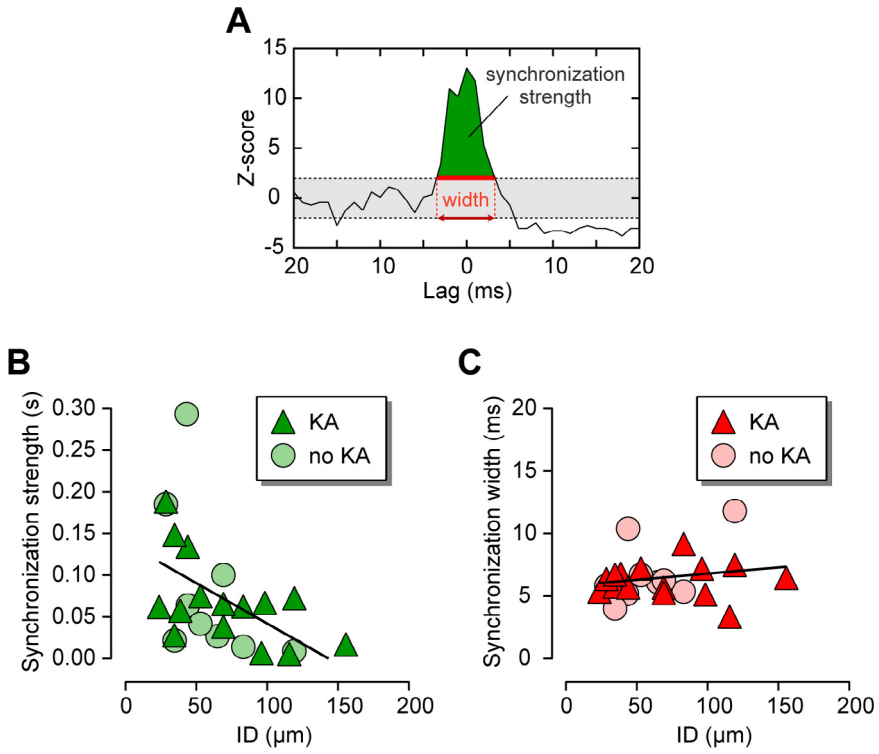

Figure S5. Synchronization of paired recorded Golgi cells.
(A) Example of a spike cross-correlogram. The synchronization width (red) is the full-width of the central peak at Z-score = 2. The synchronization strength (green) is the area of the peak above Z-score = 2. (B) and (C) Relation between the synchronization strength (B) and width (C) and the intercellular distance (ID) for paired recordings performed in the presence (triangles) or absence (circles) of kainate. Black lines are linear fits of pooled data (triangles + circles). These fits yielded regression coefficients of −0.97 ± 0.37 ms/mm (B) and 0.01 ± 0.01 ms/mm (C).

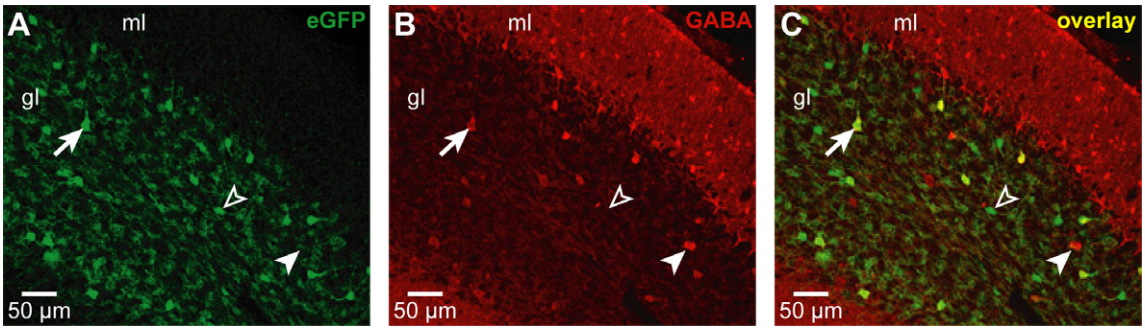

Figure S6. Immunodetection of GABA in the cerebellar cortex of GlyT2-eGFP mice.
(A) eGFP signal. Golgi cell somata and axonal periglomerular profiles are easily visible. (B) GABA staining. Some Golgi cells somata were labelled (arrow and full arrowhead). (C) Superposition of (A) and (B). Some somata were double-labelled (arrow) and some were either GABA+ (full arrowhead) or eGFP+ (empty arrowhead). gl: granular layer; ml: molecular layer. The pictures are projections from 10 confocal sections taken at 1 µm interval.

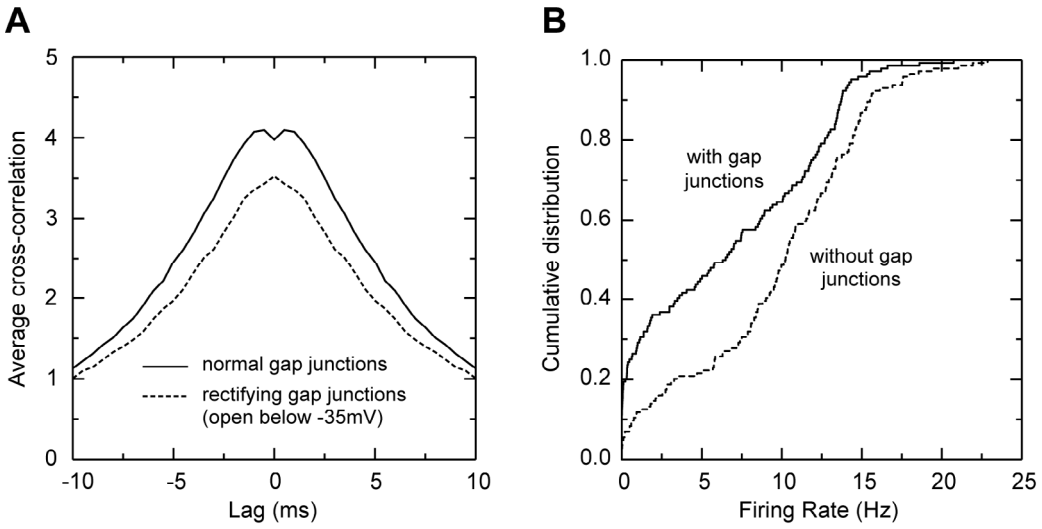

Figure S7. Effects of changing model parameters on Golgi cell population activity.
(A) Average cross-correlogram for the whole Golgi cell population in the model during sustained oscillations. Removing the depolarizing part of the electrical coupling suppresses the double peak of tight synchronisation at short latencies while leaving intact the oscillatory synchronization. (B) Electrical coupling between Golgi cells decreases the average firing frequency in the network, as expected from the hyperpolarizing effect of AHP coupling between cells (see Figure 4).

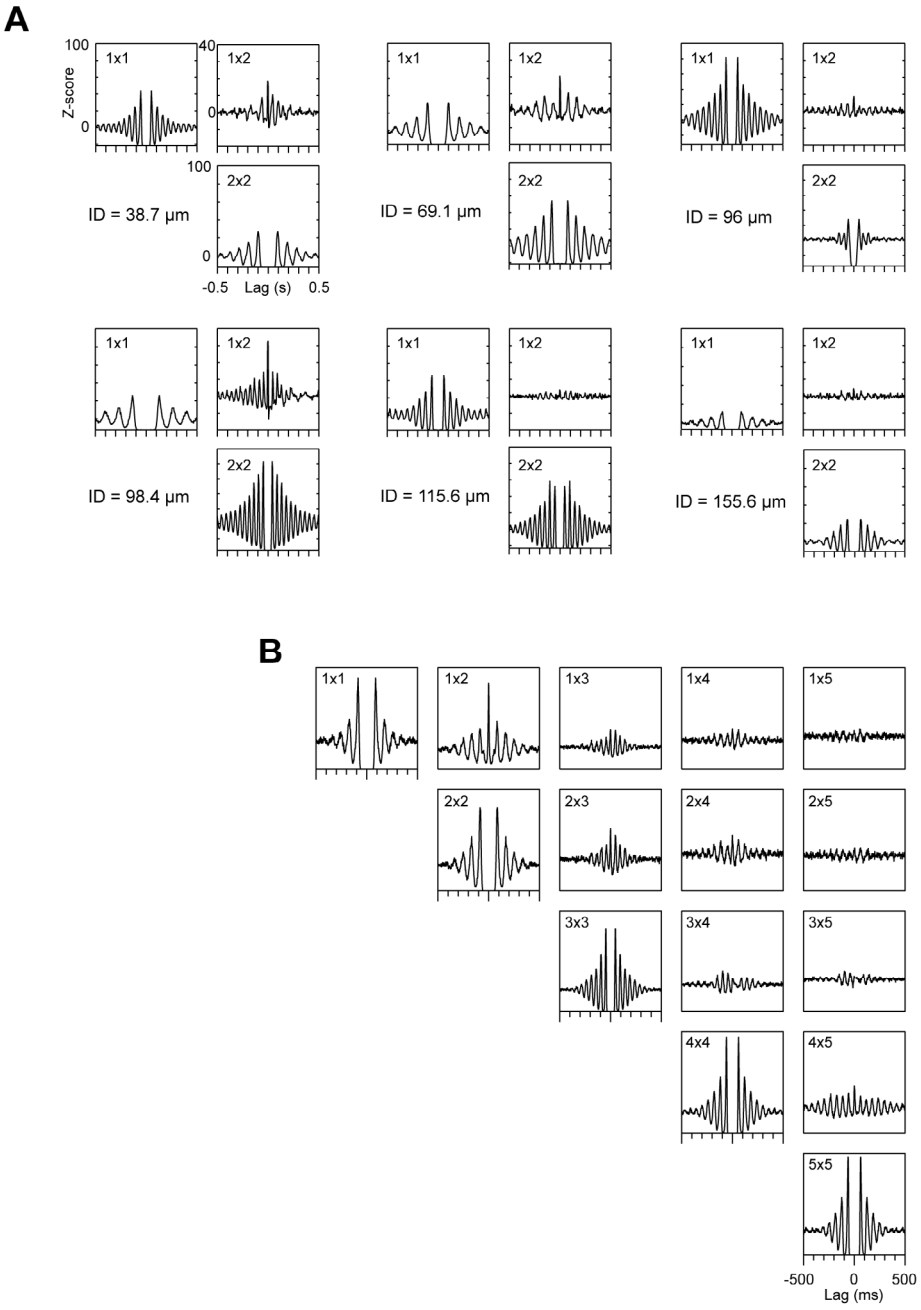

Figure S8. Correlations measured in the slice and in the model are similar.
(A) Auto-correlograms and cross-correlograms calculated from 6 cell-attached paired recordings (kainate 0.3 µM) and (B) from 5 model cells. For a given pair of cells i and j, auto-correlograms are labelled i x i and j x j, and cross-correlograms are labelled i x j. The intercellular distance (ID) is indicated for each pair in (A). In (B) the mean distance between cells i and i + 1 is 33 µm.

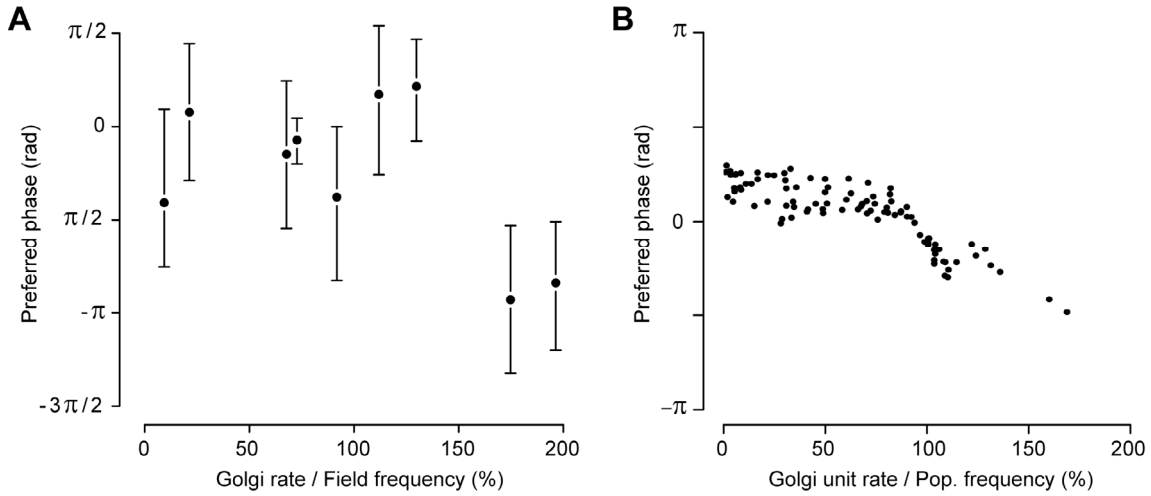

Figure S9. Golgi cells discharge with a preferred phase.
(A) Preferred phase obtained by fitting the distribution of Golgi cell spikes recorded in vivo relative to the negative peak of LFP oscillations (upward) by a von Mises circular distribution function. Predicted value and confidence intervals are indicated for the 9 units. The phase is calculated from the time of negative (upward) peaks in the filtered LFP. (B) Same plot for each individual cell of the model. The phase is calculated from the time of maximum discharge of the population which may not coincide with the reference used in A (there is no LFP in the model). Confidence intervals are not indicated in the model because their width depends mostly on the number of spikes in the sample. Note that the phase advance seen in vivo for cells discharging at higher rates is predicted by the model.